



Effect of Annealing on Microstructure and Mechanical Properties of Ultrafine-Grained Low-Carbon Medium-Manganese Steel Produced by Heavy Warm Rolling

Sohail Ahmad^{1,2} · Li-Feng Lv^{1,2} · Li-Ming Fu^{1,2} · Huan-Rong Wang³ · Wei Wang³ · Ai-Dang Shan^{1,2}

Received: 13 December 2017 / Revised: 31 May 2018 / Published online: 21 September 2018
© The Chinese Society for Metals and Springer-Verlag GmbH Germany, part of Springer Nature 2018

Abstract

An ultrafine-grained (UFG) low-carbon medium-manganese steel was fabricated by the heavily warm rolling (HWR) and subsequent quenching, and the effects of annealing temperatures on microstructure and mechanical properties of the UFG HWRed steel were investigated. The results show that the HWRed steel exhibits simultaneous improvements in strength, uniform elongation and work hardening, which is mainly attributed to the refinement of martensitic microstructures. The HWRed steels comprise only α -phase when annealing at lower temperatures below to 550 °C and at higher temperatures above to 700 °C. Whereas, UFG γ -austenite is formed by reverse transformation when the HWRed steel was annealed at intermediate temperatures from 550 to 700 °C and the volume fraction increases with increasing annealing temperatures, consequently resulting in a dramatic increase in ductility of the annealed HWRed steels. It was found that the transformed UFG austenite and ferrite remained \sim 500 nm and \sim 800 nm in size when the HWRed steel was annealed at 650 and 700 °C for 1 h, respectively, showing an excellent thermal stability. Moreover, the HWRed steel annealed at 650 °C exhibits high strength-ductility combinations with a yield strength of 906 MPa, ultimate tensile strength (UTS) of 1011 MPa, total elongation (TEL) of 51% and product of strength and elongation (PSE: UTS \times TEL) of 52 GPa%. It is believed that these excellent comprehensive mechanical properties are closely associated with the UFG austenite formation by reverse transformation and principally attributed to the transformation-induced plasticity (TRIP) effect.

Keywords Ultrafine-grained medium-Mn steel · Heavy warm rolling · Annealing · Microstructure and properties · Transformation-induced plasticity (TRIP) effect

1 Introduction

In the past decade, low-C medium-Mn transformation-induced plasticity (TRIP) steels (with Mn contents 4–12 wt%) have been paid much scientific and

technological attention due to their excellent mechanical properties with a combination of high strength and ductility [1–5]. Miller comprehensively studied the medium-Mn TRIP steel (Fe–0.11C–5.7Mn) by intercritical annealing treatment and received a good combination of UTS 878 MPa and TEL 34% [11]. After his work, a series of researches were carried out on low-C medium-Mn steels to optimize the mechanical properties through intercritical annealing processing to obtain stable ultrafine-grained (UFG) austenite by reverse transformation [6–12].

Microstructure or grain refinement is an effective way to improve both strength and ductility of the steels [3, 9, 10, 12–15]. To fabricate the nano-grained (NG) and ultrafine-grained (UFG) materials by conventional severe plastic deformation (SPD), such as equal channel angular pressing (ECAP), accumulative roll bonding (ARB) and high-pressure torsion (HPT), has attracted a great attention over the past half century [16–19]. Unfortunately, the UFG

Available online at <http://link.springer.com/journal/40195>

✉ Li-Ming Fu
lmfu@sjtu.edu.cn

✉ Ai-Dang Shan
adshan@sjtu.edu.cn

¹ School of Materials Science and Engineering, Shanghai Jiao Tong University, Shanghai 200240, China

² Collaborative Innovation Center for Advanced Ship and Deep-Sea Exploration (CISSE), Shanghai 200240, China

³ Baosteel Research Institute, Shanghai 201900, China

steels prepared by these SPD techniques are usually at laboratory scale, which greatly limit their extensively industrial applications. Rolling is the most suitable way to produce larger sheets or/and plate-type materials. Most recently, thermomechanical processing method such as hot rolling with subsequent quenching and/or tempering (Q&T), combining plastic deformation and phase transformation manipulation, is applied in producing large-scale fine-grained medium-manganese steels [4–6, 20–22]. Furthermore, it is reported that cold rolling followed by subsequent annealing or austenite reverted transformation annealing (ART) has also been utilized to successfully fabricate the ultrafine-microstructured multi-phase medium-Mn steels [2, 7, 10, 13, 14]. However, it should be noted that conventional hot rolling technique is generally difficult to achieve the ultrafine-grained steels with an effective grain size below 1 μm owing to extensively dynamic recovery and recrystallization at high-temperature deformation. The severe cold rolling process is also rarely used to prepare nano- or ultrafine-grained high strength steels due to the strong resistance of deformation. In comparison, warm rolling processing is normally performed in the temperature region of 500–800 $^{\circ}\text{C}$ and provides a feasible way to produce UFG materials in steel industry [23]. It is well known that the warm deformation of the undercooled austenite phase prior to martensite transformation, so-called ausforming technique, has been proved to be effective in refining the subsequent transformed martensite structures [24, 25]. Warm rolling processing with the subsequent microstructures manipulating by heat treating has been intensively used for refining plain carbon steels [26, 27]. Recently, studies have also shown that the medium-manganese steel can achieve ultrafine microstructure by warm rolling method followed by reverted transformation annealing, and consequently realizing the excellent comprehensive properties with high strength and high ductility balance [28–30]. However, few works have been undertaken to systematically study the annealing effect on the heavily warm-rolled low-C medium-Mn steel.

In this article, we aim to produce UFG low-C medium-Mn steel through heavily warm rolling and subsequent annealing treatment. The effect of annealing temperatures on the microstructure and mechanical properties of heavily warm-rolled steel was studied systematically, and the deformation behavior and strengthening mechanism were also discussed in the article.

2 Materials and Experimental Procedure

The material investigated in this study is hot-rolled steel provided by Baosteel Research Institute, China. The chemical composition of the steel is given in Table 1. The as-received plate with a thickness of 20 mm was firstly austenitized at 900 $^{\circ}\text{C}$ for 1 h and hot rolled (HRed) into 6.5 mm in thickness by five passes with a reduction of 67.5% followed by quenching. The obtained steel was cut into small plates with a dimension of 120 mm in length and 20 mm in width. The small plates were annealed at 870 $^{\circ}\text{C}$ for 1 h, air-cooled to 650 $^{\circ}\text{C}$ and then further heavily warm rolled (HWRed) to a thickness of 1.95 mm with a reduction ratio of 70% by 2 passes. The finishing HWR temperature was 550 $^{\circ}\text{C}$ and then followed by water quenching. The HWRed steel samples were annealed at 400, 500, 550, 580, 600, 620, 650, 700, 750, 800 and 900 $^{\circ}\text{C}$ for 1 h, respectively, followed by air cooling to room temperature (RT). The schematic diagrams of HWR processing and orientations of warm-rolled samples are as illustrated in Fig. 1a, b, respectively. The rolling, the normal and the transverse directions of the HWRed plates are abbreviated as RD, ND and TD, respectively.

X-ray diffraction (XRD) measurements were performed to identify the coexisting phases in the samples and to determine the austenite fraction by using Shimadzu XRD-6000 diffraction instrument with $\text{CuK}\alpha$ radiation and a wavelength of 0.1540562 nm at 40 kV and 30 mA. The samples were scanned from 30 $^{\circ}$ to 100 $^{\circ}$ at a scanning speed of 1 $^{\circ}$ /min. The XRD samples were electrochemically polished in a solution of 5% HClO_4 and 95% $\text{C}_2\text{H}_5\text{OH}$ before measurements to eliminate the effect of mechanical polishing and cutting. The austenite volume fraction (V_A) at different conditions was evaluated on the basis of the following equation [31–33].

$$V_A = \frac{1.4I_\gamma}{I_\alpha + 1.4I_\gamma}, \quad (1)$$

where I_γ and I_α are the integrated intensities of the austenite and ferrite, respectively. In this study, the integrated intensities of $\gamma(200)$, $\gamma(220)$, $\gamma(311)$, $\alpha(200)$ and $\alpha(211)$ peaks were used to determine V_A [32].

The samples for scanning electron microscopy (SEM) were mechanically polished and etched in a 4% HNO_3 and 96% $\text{C}_2\text{H}_5\text{OH}$ solution. The SEM was performed using JEOL-7600F with an operating voltage 15 kV along ND–RD plane. The transmission electron microscopy (TEM) was performed with JEM-2100F operating at 200 kV. The

Table 1 Chemical composition of experimental steel (wt%)

C	Si	Mn	Al
0.15	0.3	7.0	1.0

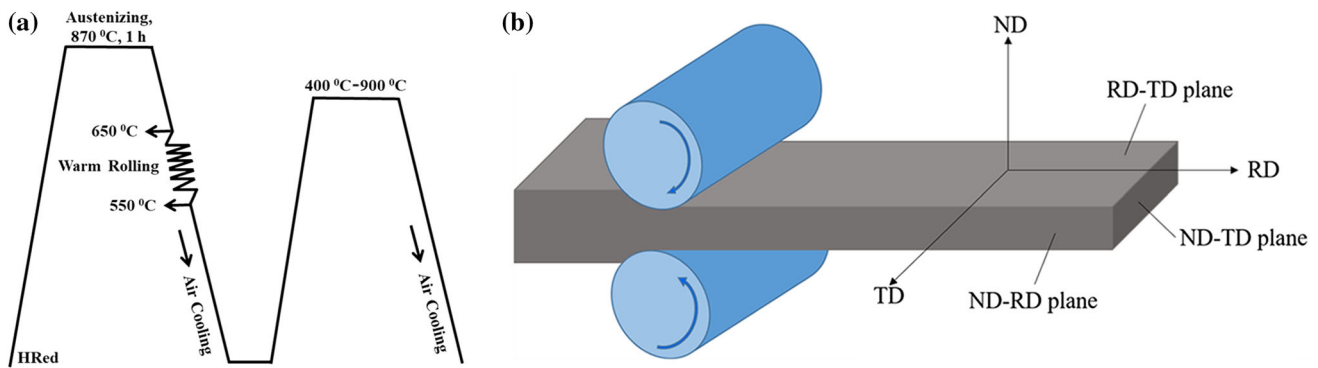


Fig. 1 **a** Schematic diagram for warm rolling process, **b** illustration of directions of warm-rolled sample

thin foils for TEM observations were obtained by a twin-jet electro-polisher operating at 50 V, 30 mA in a solution containing 5% HClO₄ and 95% C₂H₅OH at -25 °C.

A Buehler Micromet Hardness Tester, with a Vickers pyramid indenter-keeping load of 1 kg and dwell time of 15 s, was used to measure the microhardness (HV) along ND-TD, ND-RD and RD-TD planes. The average of seven measurements was finally taken as an effective value of the hardness for each sample. The flat specimens were longitudinally cut along RD direction for tensile testing. The gauge length, width and thickness of the samples were 12, 4 and 2 mm, respectively. Tensile tests were conducted on the Zwick/Roell z100 tensile tester at a strain rate of $5 \times 10^{-4} \text{ s}^{-1}$ at room temperature.

3 Results

3.1 Microstructure Evolution

XRD patterns of the specimens at different conditions (HRed, HWRed and annealed at various temperatures) before and after tensile testing are presented in Fig. 2a, b,

respectively. The analysis from Fig. 2a shows that HRed and HWRed steels before tensile are composed of only α -phase and maintained stable below annealing temperature at 550 °C. It is found that the HWRed that annealed from 550 to 700 °C contains γ phase peaks and the relative intensity markedly enhanced with the increasing annealing temperature, implying the occurrence of reverse austenite transformation during the intercritical annealing temperature range. Moreover, the austenite peaks $\gamma(111)$ and $\gamma(200)$ are more intense for HWRed steel annealed at 700 °C than annealed at any other lower temperature. In contrast, the diffraction peaks are obviously broadened for steels after tensile, which is probably due to the residual stresses and high dislocation density induced by the deformation. Moreover, γ phase peaks are also clearly found in the tensioned samples annealed from 580 to 700 °C but the relative intensity ratio of the $(111)\gamma$ and $(110)\alpha$ peaks is greatly reduced, as shown in Fig. 2b. Evidently, strain-induced martensite (SIM) transformation ($\gamma \rightarrow \alpha'$) occurs, and TRIP effect dominates the processes of the tensile deformation. Moreover, it should be noted that the γ phase is transformed incompletely and still remains a certain amount in the annealed samples even after tensile testing,

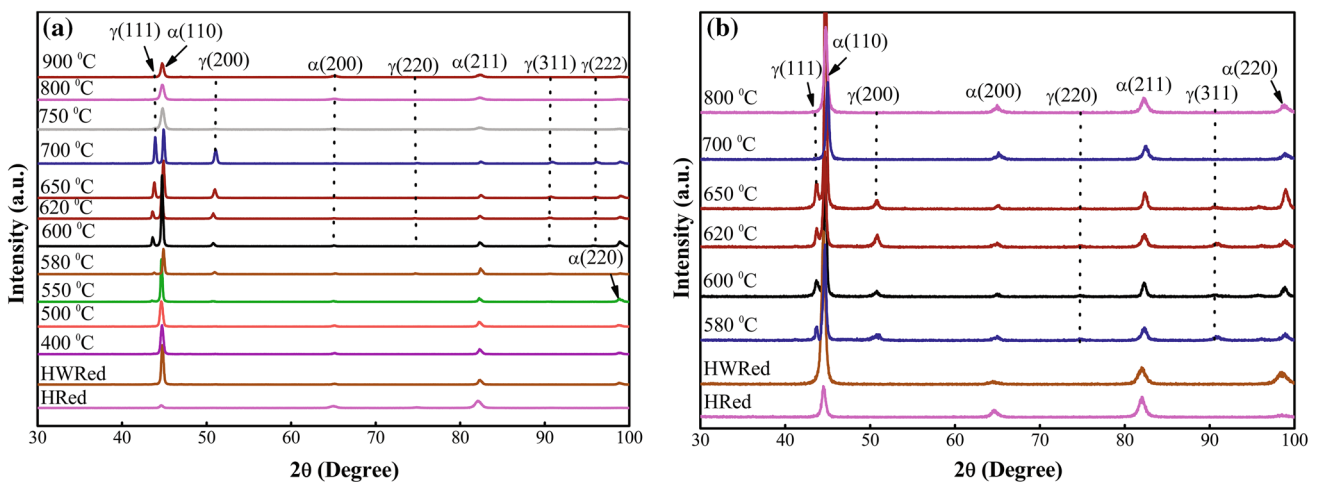


Fig. 2 XRD patterns of experimental steels before **a**, after **b** tensile tests at different annealing temperatures with annealing time of 1 h

which indicates that the newly formed austenite by HWR and subsequent reverse transformation possesses relatively mechanical stability. Figure 3 presents the change in measured volume fraction before and after tensile as a function of annealing temperatures from 580 to 700 °C. It is shown that the austenite volume fraction of the steel before tensile increases monotonically from 15% at 580 °C to 55% at 700 °C. Whereas, the volume fraction of the steel after tensile is greatly reduced with increasing annealing temperature. It first increases from 10% at 580 °C to the ultimate 21% at 620 °C and then declines to 4% at 700 °C. Noticeably, the transformation ratio of the austenite increased monotonically with increasing annealing temperature although the amount of the austenite for SIM transformation was relatively small in the samples of lower annealing temperatures below 650 °C, as shown in Fig. 3.

Figure 4 displays typical SEM images of medium-Mn steel at different conditions. The HRed steel exhibits a typical lath martensite microstructures (Fig. 4a). Generally, conventional martensite morphology is characterized by packets, blocks and laths that hierarchically transformed from equiaxed coarse parent austenite grains. However, in comparison, the martensitic structures for the steel after heavily warm rolling are extensively refined and present an obvious ultrafine lamellar plates comprising only laths, as shown in Fig. 4b, which are quite similar to the observations in the other warmly deformed medium-manganese steels reported in Refs. [30, 34]. Moreover, the detailed substructure inside the lamellar plate cannot be clearly defined in SEM images. It is believed that these microstructure characteristics are closely associated with the martensite phase transformations from the deformed elongated austenite during heavy warm rolling and subsequent quenching. Figure 4c–f shows the microstructures of the HWRed samples annealed at 600, 650, 700 and 800 °C, respectively. The annealing treatment at 600, 650, 700 °C

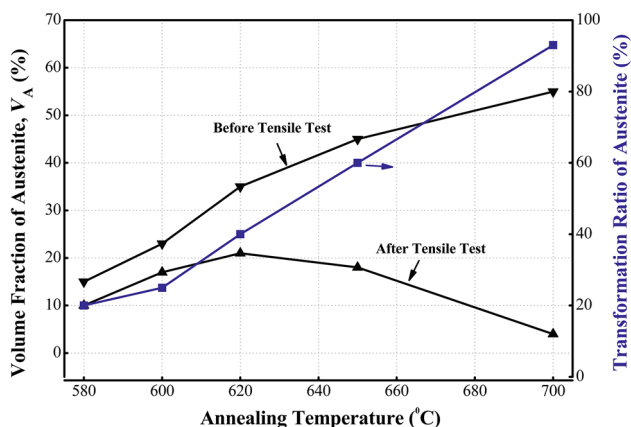


Fig. 3 Measured austenite fraction and transformation ratio for the samples before and after tensile testing at different annealing temperatures

on HWRed steel resulted into the formation of blocky ultrafine-grained ferrite and austenite (as indicated by arrows) and the size of these block phase increases with increasing annealing temperature. According to the above analysis, the austenite phase can form by reverse transformation during annealing at intermediate temperatures. The 800 °C is above the A3 temperature (775.7 °C), and HWRed steel at or/and after 800 °C annealing and subsequent quenching contains comparably larger size martensitic plates, as seen in Fig. 4f.

Detailed microstructures of the experimental steels at different conditions are examined by TEM, as shown in Fig. 5. In comparison with the coarse martensite plates of the HRed steel in Fig. 5a, the HWRed steel in Fig. 5b exhibits the refined microstructures with dense tangled dislocations and dislocation cells. The warm rolling can definitely strengthen the undercooled austenite by refining the austenite grains and by introducing a large number of dislocations into it, consequently resulted in the final refinement of the martensite plates [24, 28–30]. The intercritical annealing was performed to push the inversely transformation of the martensite into austenite. Figure 5c–f demonstrates the typical TEM images of the HWRed steel annealed at 600, 650 and 700 °C, respectively. The equiaxed ultrafine microstructures are clearly observed, and the grain size increased gradually with increasing annealing temperature. According to XRD analysis in Fig. 2 and SEM examination in Fig. 4, these ultrafine microstructures are austenite and ferrite, as indicated by the arrows in Fig. 5d. The inset in Fig. 5d shows the diffraction pattern of austenite phase indicated by arrow. The dark field (DF) and the diffraction rings also proved the presence of equiaxed UFGs of austenite in the structures shown in Fig. 5e. The selected area diffraction (SAED) pattern exhibits the typical continuous rings, which are the characteristics of UFGs [35] separated by boundaries having high angle of misorientation. Furthermore, the UFG austenite and ferrite newly formed by transformation still remain below 500 nm and 800 nm in size at 650 and 700 °C annealing, respectively, indicating considerable thermal stability.

3.2 Mechanical Properties

Figure 6 presents the variation of microhardness (HVs) of the annealed HWRed steel along three different planes at various annealing temperatures. The hardness of HWRed sample is improved along all the planes as compared to HRed sample. The change in hardness on different planes is small at a fixed annealing temperature, i.e., $HV_{ND-TD} \approx HV_{ND-RD} \approx HV_{RD-TD}$, indicating that the mechanical properties of the material are uniform and no obvious anisotropy exists in this steel. The microhardness of the samples decreases as the annealing temperature rises from

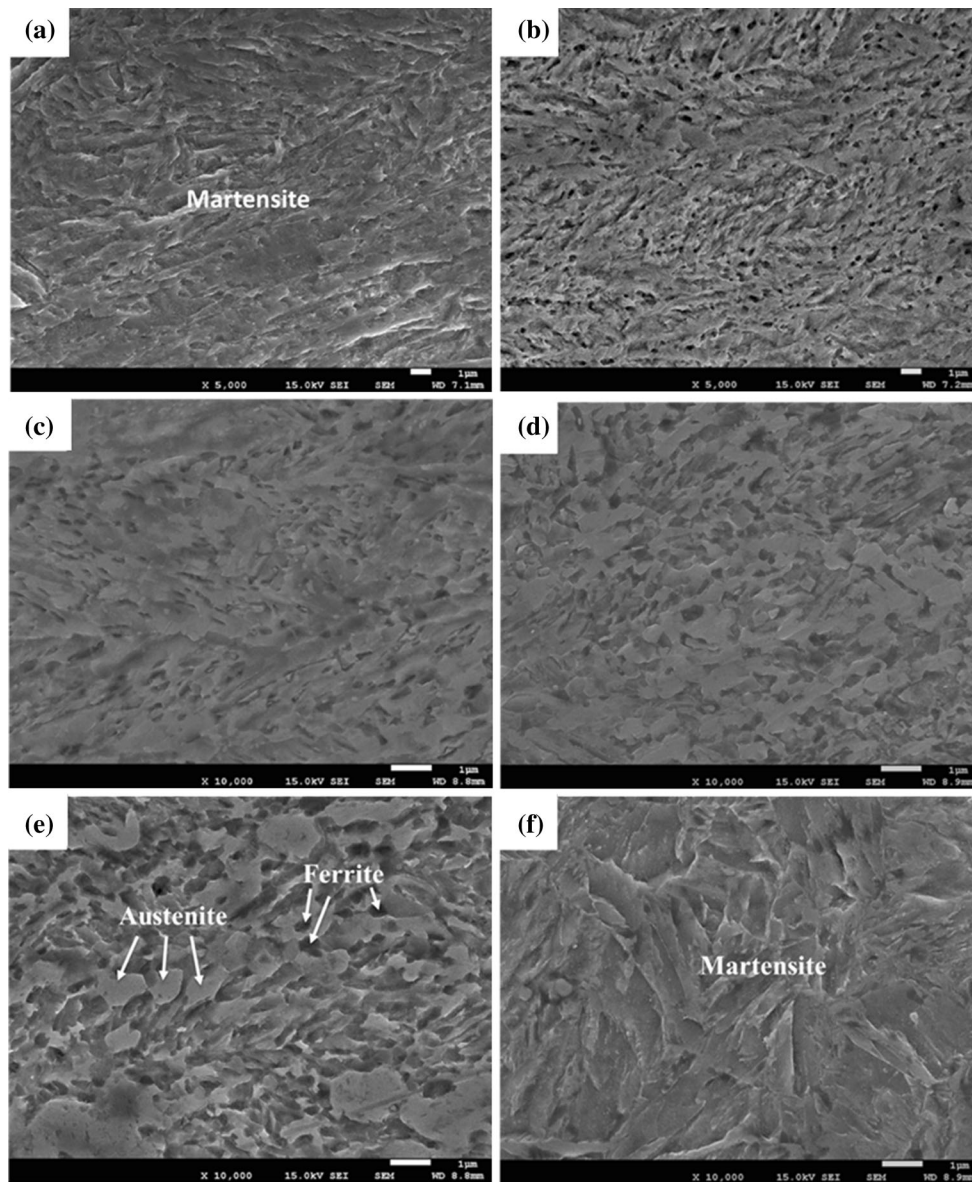


Fig. 4 SEM images of experimental steels along ND–RD plane: **a** HRRed, **b** HWRed, **c** annealing at 600 °C, **d** annealing at 650 °C, **e** annealing at 700 °C, **f** annealing at 800 °C at annealing time of 1 h followed by air cooling

400 to 700 °C, which result from the recovery and recrystallization of the deformed microstructures and the soft phase formation of ferrite and austenite. The microhardness has an abrupt increase at 750 °C annealing and then rapidly decreases with annealing temperatures. An abrupt increase in hardness is due to martensite transformation from the nearly fully austenitized HWRed steel by annealing near A3 temperature and quenching, while the subsequent decrease in hardness should be attributed to martensite structures coarsening resulting from the grain growth of the prior austenite at higher annealing temperatures. Figure 7 demonstrates the representative tensile stress–strain (σ – ϵ) curves of studied steels at different conditions. The corresponding yield strength (YS), ultimate

tensile strength (UTS), total elongation (TEL) and product of strength and elongation (PSE) values for HRRed, HWRed and annealed samples are given in Table 2. The HWRed steel shows an enhancement in both YS and UTS as well as better work hardening ability in comparison to the HRRed steel. Annealing treating reduces the strength but increases the ductility and elongation of the HWRed steel to some extent. In particular, the PSE and TEL of the 650 °C annealed steel are about 3 and 5 times higher than those of HWRed steel, respectively, as listed in Table 2. It was found that the HWRed steel at different annealing temperatures exhibits very different tensile behaviors. The HWRed sample annealed at 600 and 650 °C shows a discontinuous yielding phenomenon with large yielding

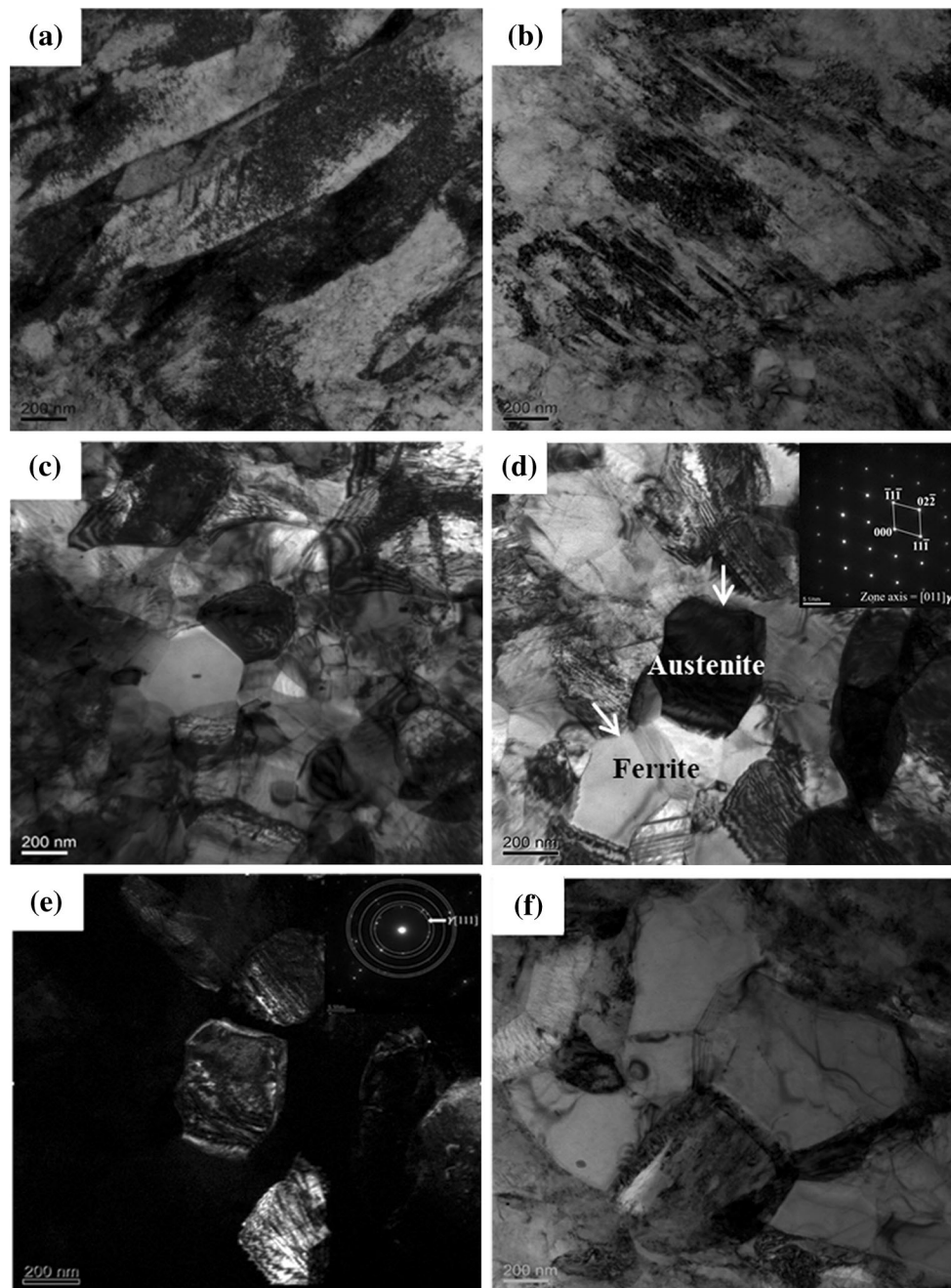


Fig. 5 Typical TEM images of experimental steels: **a** HRRed, **b** HWRed, **c** annealing at 600 °C, **d** bright field (BF) image of the sample annealed at 650 °C, the inset showing diffraction pattern of austenite indicated by arrow, **e** dark field image of γ phase corresponding to (111) crystal plane of BF image in **d**, the inset showing the selected area diffraction pattern (SAED), **f** annealing at 700 °C for 1 h followed by air cooling

plateau; especially the sample annealed at 650 °C, the yielding plateau maintains almost the entire macroscopic tensile process with a remarkable yield elongation of 51%. Whereas, for the HWRed steel annealed at 700 °C, the tensile curve only presents an obviously large yielding plateau at the initial plastic deformation stage, followed by a rapid work hardening. We believe that these phenomena are principally associated with the austenite formation in reverse transformation.

The strain hardening rates (SHR) as a function of true strain for experimental samples containing austenite and no austenite are illustrated in Fig. 8a, b, respectively. It is clear that the SHR decreases monotonically with increasing true strain after fluctuations at the early stage of deformation for all samples (Fig. 8a). The HWRed and 750 °C annealed steel has a higher strain hardening rate than that of the HRRed steel. It is evident from Fig. 8b that the samples with higher austenite fraction seem to be higher

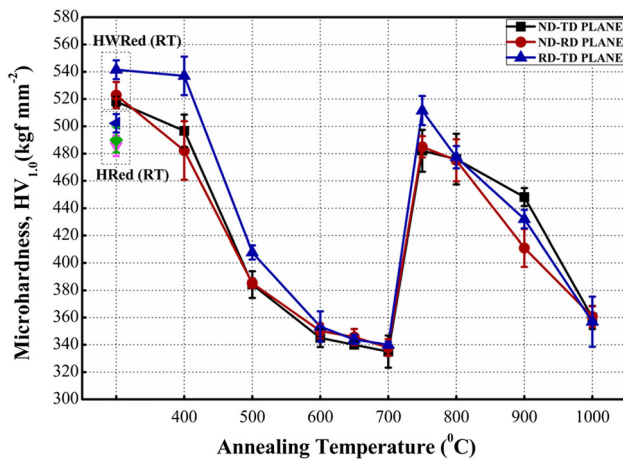


Fig. 6 Variation of microhardness HV values with annealing temperature along ND–TD, ND–RD and RD–TD planes for annealing time of 1 h followed by air cooling

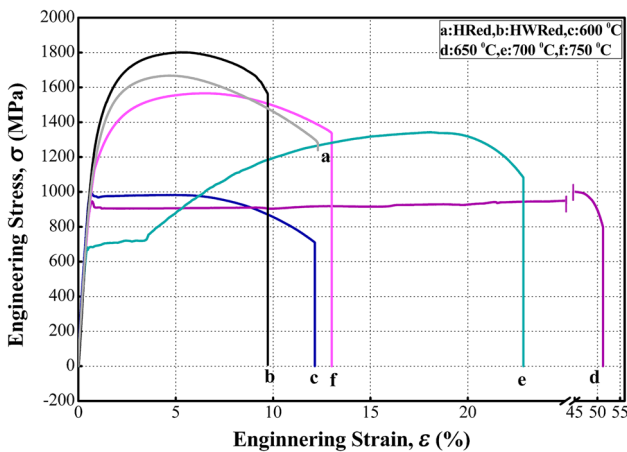


Fig. 7 Typical tensile stress–strain (σ – ϵ) curves of annealed experimental steels at different annealing temperatures for 1 h followed by air cooling

SHR according to the results from Fig. 3. In addition, on the basis of characteristics of the strain hardening rates and the tensile curves with special yielding phenomenon (Fig. 8b), it can be readily divided into four stages as indicated by 1, 2, 3 and 4 for the curve of 650 °C annealed sample. (Similar scheme is applied to other curves.) The SHR decreases rapidly in the stage 1, and then increases sharply in the stage 2. Some fluctuations are found with

unequal amplitudes between the stage 1 and 2 for 700 °C annealed sample. SHR of 600 °C annealed sample slightly decreases in the stage 3, and then increases at about 7% true strain and then decreases again. SHR of 650 °C annealed sample remains almost constant above and near the zero level in the stage 3 with little fluctuations. Similarly, SHR of 700 °C annealed sample decreases with large number of fluctuations above the zero level in the stage 3. It is believed that all of these changes are directly related to the austenite, which will be discussed later.

Figure 9 displays the SEM images of the fracture analysis of low-C medium-Mn steel. It is obvious that the failure of all the specimens mainly exhibits ductile characteristics with dimples. Comparably, the dimples’ size of HRed sample is larger than those of other samples. A uniform distribution of the dimples can be observed throughout the fracture surface of HWRed and HWRed steel annealed at 650 °C due to the presence of UFGs. Beside of most of ductile dimples, some cleavage facets are also observed in the HRWed steel and the 700 °C annealed steel, as shown in Fig. 9a, d, implying that the steels present some degree of brittleness although the main fracture mode is dominantly ductile. The 650 °C annealed sample shows bigger and deeper surface inside the dimples in comparison with other samples, confirming the more ductile behavior of this sample. The fracture mechanism is believed to be the martensitic cracking during straining for HRed and HWRed samples, whereas it is less frequent in the case of 650 °C and 700 °C annealed samples because voids are formed primarily at the ferrite–austenite interface, and distributed uniformly until the fracture occurs. Furthermore, the transgranular fracture was observed in all of these samples, which is associated with the dimples.

4 Discussion

4.1 Heat Treatment and Its Effect on Microstructure Evolution of HWRed Steel

Compared with hot-rolled and quenched steel, the HWRed steel exhibits a refinement of the martensitic microstructures. Generally, warm deformation of the metastable or

Table 2 Typical tensile properties of experimental steels

States	YS (MPa)	UTS (MPa)	TEL (%)	PSE (GPa%)
HRed steel	1232.2 ± 3.5	1667.5 ± 10.5	12.3 ± 0.8	20.5 ± 1.5
HWRed steel	1380.7 ± 4.7	1801.7 ± 9.7	9.7 ± 0.6	17.5 ± 1.2
600 °C/h	976.4 ± 3.3	995.2 ± 7.4	12.1 ± 0.4	12.1 ± 0.5
650 °C/h	905.8 ± 4.7	1011.4 ± 6.5	51.2 ± 2.1	51.8 ± 2.5
700 °C/h	683.9 ± 5.4	1342.3 ± 10.2	22.3 ± 1.4	29.9 ± 2.1
750 °C/h	1028.4 ± 7.9	1566.7 ± 9.8	13.1 ± 0.7	20.5 ± 1.2

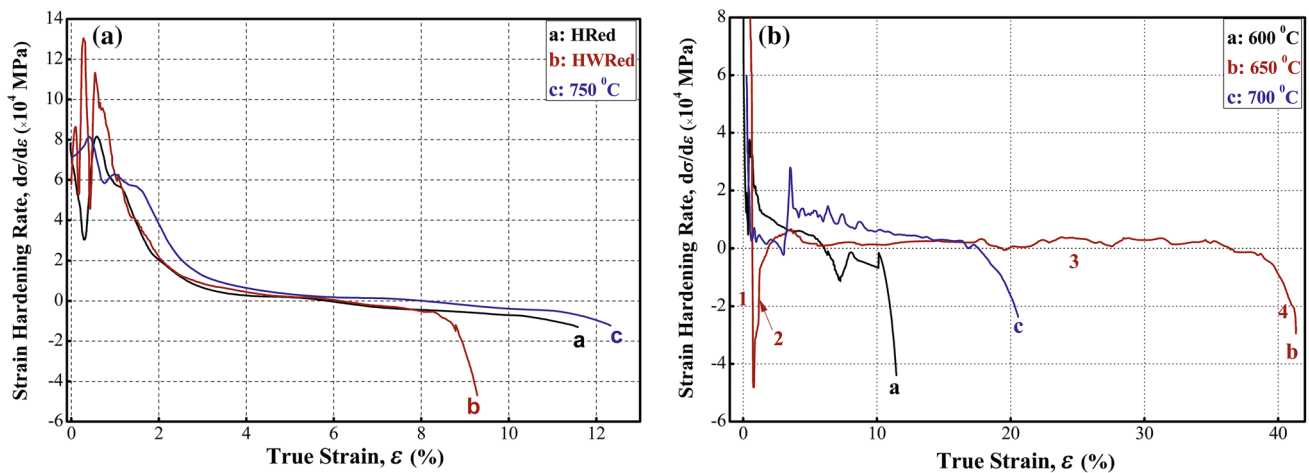


Fig. 8 Variation of strain hardening rate (SHR) of experimental steel with true strain: **a** samples without austenite, **b** samples with austenite

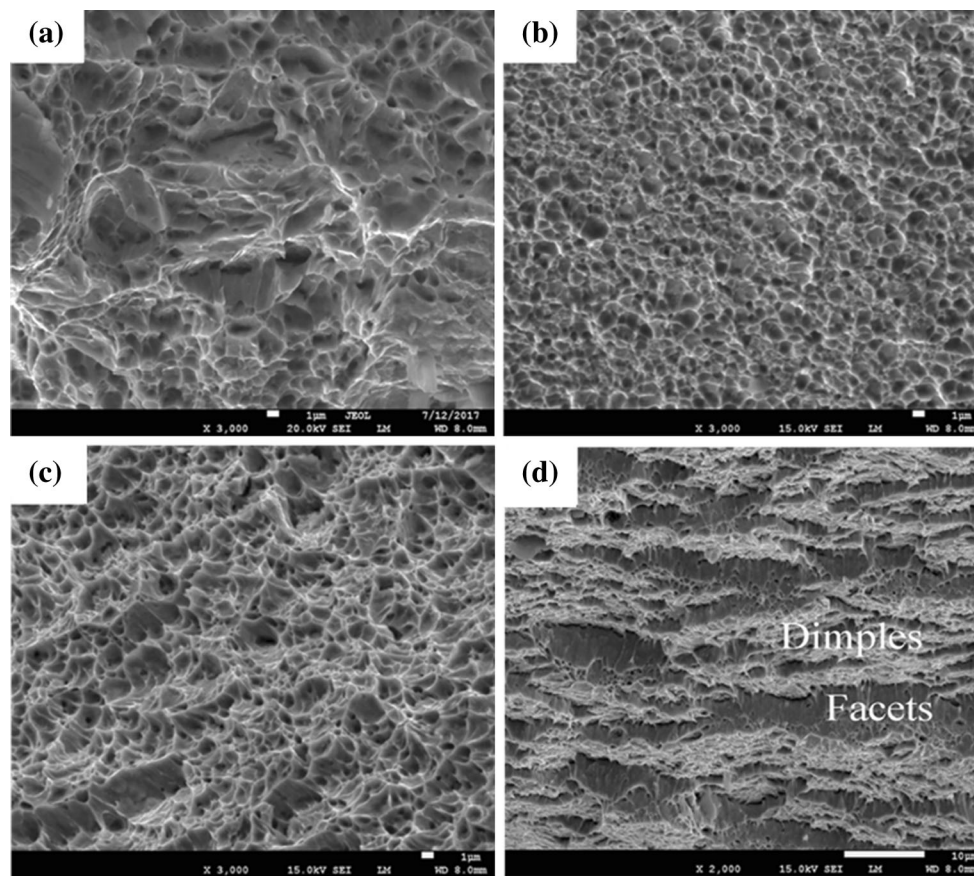


Fig. 9 SEM images of fracture surface of experimental steels in different processing states: **a** HRRed; **b** HWRed; **c** annealing at 650 °C, **d** annealing at 700 °C

undercooled austenite phase prior to martensite transformation inhibits the occurrence of extensive austenite recovery and recrystallization and elongates the austenite and results in the formation of lamellar martensite structure after quenching, consequently prevents the coarsening of transformed martensite [24, 26, 29]. Therefore, the warm

rolling process plays a very important role in microstructure manipulating. Figure 10a illustrates the CCT diagram of experimental steel predicted by JMatpro database. According to the CCT diagram, the transformation time of ferrite is 13 min at a temperature of 550 °C with the critical cooling rate of 0.8 °C/s, which is much longer than the

cooling and warm rolling processes. Therefore, the heavily warm rolling process in this study was carried out in a region containing only metastable or undercooled austenite phase and the ferrite transformation will not occur. Moreover, the upper transformation temperatures of pearlite and bainite are both below the finish rolling temperature (550 °C). Therefore, the undercooled austenite can be plastically deformed without the occurrence of phase transformation on the basis of the CCT diagram and the processing parameters of warm rolling in the present study. Once the heavily warm rolling process was completed, the deformed metastable austenite with high density defects on subsequent quenching became unstable and transformed to martensite at M_s and transformation completed at M_f . Martensite is recognized as the supersaturated solution of carbon and is believed to be important strengthening phase. The transformation from face-centered cubic austenite to fully strained body-centered tetragonal martensite is a type of shear deformation. Moreover, HWR process results in the refinement of the microstructures of metastable austenite with high density of defects, such as dislocations, dislocation cells and dislocation networks [29], which will greatly contribute to the martensitic microstructure.

Through warm deformation and heat treatment, the microstructures of the medium-manganese steels can be effectively manipulated [36–38]. The present results show that the microstructures of HWRed steel annealed at below 550 °C and at above 700 °C comprise only α -phase. However, the microstructure of HWRed steel annealed at intermediate annealing temperature from 550 to 700 °C comprises γ -austenite and α -phases, due to reverse transformation. The formation of equiaxed and blocky microstructure of γ -austenite and α -phases at 600–700 °C annealing treatment (Figs. 4, 5) indicates the completion of recrystallization process. To manipulate the austenite

formation by HWR and annealing plays an important role in fabrication of high strength-ductility UFG low-carbon medium-Mn steels. In this study, it was found that the volume of UFG austenite can be obtained from 15% at 580 °C annealing to 55% at 700 °C annealing due to the fact that the high annealing temperature facilitates the growth and formation of the austenite. It is well established that retained austenite mechanical stability is directly proportional to its C concentration [37]. The C concentration should be low at higher annealing temperatures in the present case, consequently more austenite transformed to martensite during tensile testing (see Fig. 3). Figure 10b illustrates the phase fraction of experimental steel predicted by JMatpro database. It can be observed that the austenite fraction increases with increasing annealing temperature. The 52% V_A at 650 °C and 70% at 700 °C balanced with the ferrite are completely in accordance with the trend observed and obtained V_A results at different annealing temperatures. Some cementite particles (about 1%) were also observed in the temperature range of 530–610 °C. Moreover, the formation of constituent's phases in steels greatly depends upon the annealing temperatures [39, 40]. The ferrite formed at the austenite grain boundaries, whereas the austenite grains nucleated and grew at lath boundaries, within laths and at martensite packet boundaries. Consequently, the abundant amounts of austenite nucleation sites were formed in the martensitic structure during the annealing process.

4.2 Effect of Annealing on Mechanical Properties of HWRed Steel

It is believed that the enhancement in HV, YS and UTS of HWRed steel in comparison with those of HRed steel is greatly attributed to refined lamella plates of martensite

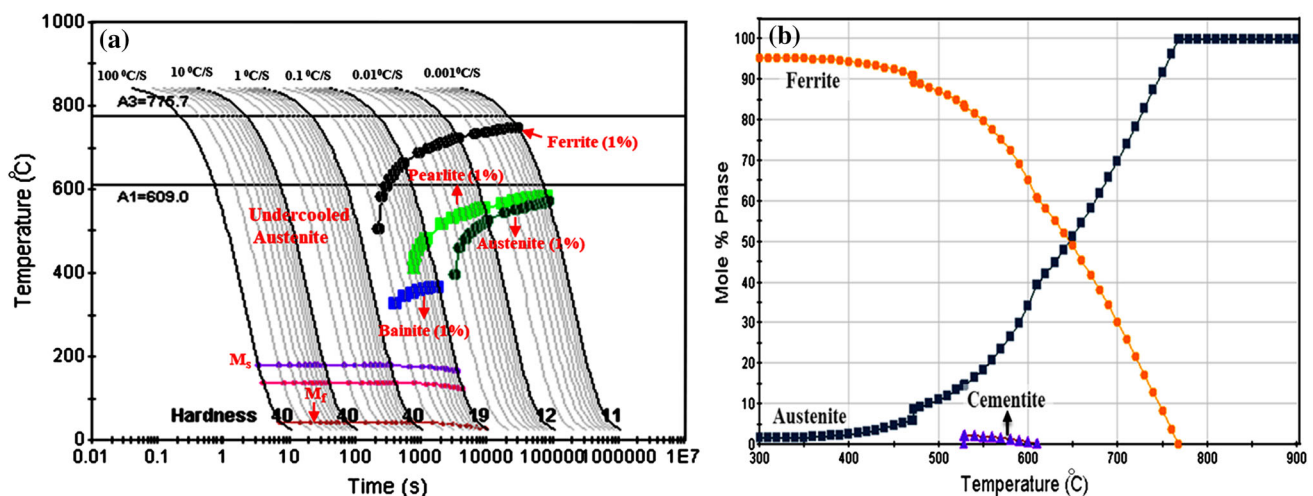


Fig. 10 a CCT diagram, b phase fraction of experimental steel, predicted by JMatpro database

microstructure having dense tangled dislocations and dislocation cells. Mechanical properties are significantly affected by the annealing temperature because of varying ferrite and austenite volume fractions. The annealing treatment at 400–700 °C for HWRed steel causes the decrease in HV. This should be mainly attributed to the recovery or recrystallization of grains during heat treatment and the formation of newly equiaxed soft phase of austenite by reverse transformation (Figs. 3, 5). The increase in HV exponentially from 700 to 750 °C is, however, attributed to the formation of martensite phase. Similarly, the decrease in HV beyond 750 °C corresponds to the formation of larger size martensite plates. It can be seen from Table 2 that annealing at 600 °C results in the decrease in the values of YS and UTS in comparison with those of HWRed steel. This is because of the introduction of soft austenite phase into the microstructure. The gradual decrease in YS in the temperature range 600–700 °C is mainly because of the increase in austenite volume fraction, whereas YS rebounds at 750 °C because of the presence of martensite fraction. Similarly, increase in UTS in the temperature range 600–700 °C is believed due to enhanced TRIP effect induced during tensile deformation [41], whereas further increase in UTS at 750 °C is attributed to the introduction of the martensite phase [2, 13, 36]. Moreover, better strength-elongation combination of HWRed steel at 650 °C may be attributed to the grain refinement and enhanced TRIP effect [12, 13].

The enhancements in HV, YS and UTS of HWRed steel as compared to those of HRed steel are partially attributed to grain boundary strengthening mechanism in the present study. Generally, grain boundary strengthening mechanism is described by Hall–Petch equation [36].

$$\sigma_Y = \sigma_0 + k_Y d^{-1/2}, \quad (2)$$

where σ_Y is yield strength, σ_0 is frictional stress, k_Y is Hall–Petch constant and d is the average grain diameter. Similarly, when it needs to describe the relationship between HV and d , the yield strength σ_Y is replaced by the microhardness HV in Hall–Petch equation. The modified equation is given below [42].

$$HV = H_0 + k_H d^{-1/2}. \quad (3)$$

Both k_H and H_0 are constants and are associated with HV measurements. The SEM and TEM observations have demonstrated that the microstructure was refined for HWRed steel. It is also well known that the decrease in grain size enhances the resistance for dislocation motion at the grain boundary (GB), therefore improves the yield stress. Similarly, the hardness would be high if more stress is required to move the dislocations across GB [43]. Evidently, grain boundary strengthening mechanism is a major

cause in strengthening the HWRed steel and annealed HWRed steels at the temperatures from 600 to 700 °C.

Generally, the relationship between HV and YS satisfies [43]:

$$HV = c\sigma_Y, \quad (4)$$

where HV and YS are measured in kgf/mm^2 and MPa, respectively, c is the elastic constraint factor and usually estimated to be 0.3 by using blunt pyramid indenters [44]. In the present study, using HV along ND–RD plane, the value of c for HWRed steel annealing at 600 and 650 °C is measured to be 0.3, whereas its value, for HRed and HWRed steels, is measured to be 0.39 and 0.40, respectively. As HV and YS are directly affected by the microstructure, the relationship between them should also be affected by the microstructure. The relationship of HV and YS is supposed to be affected by high dislocation density, which became a cause of larger value of c in this study.

The higher SHR for HWRed steel in comparison with that of HRed steel is attributed to the refinement of the microstructure due to HWR. The curves in Fig. 8a decrease monotonically with the true strain after some fluctuations at the early stage of deformation near the yield point. It is well known that SHR is closely related to the amount and mechanical stability of the austenite. The transformation ratio of the austenite increases with increasing annealing temperature from 580 to 700 °C. In addition, the grain size of the newly formed austenite also increases with rising annealing temperature. These result in a significant decrease in the mechanical stability of the austenite. The occurrence of SIM transformation and TRIP effect during tensile deformation will greatly improve SHR in this temperature range. The rapid decrease trend of SHR in stage 1 exhibited in Fig. 8b should be attributed to an inhomogeneous strain partitioning between the ferrite, austenite and martensite [10, 13, 34] and dynamic recovery of dislocations in initial plastic stage [45]. The variation of SHR at the stage 2 and 3 is mainly characterized by enhanced TRIP effect. Usually, SIM transformation involves two aspects. One is a softening effect due to the strain energy consumption for martensite formation, which will lead to the stress reducing with strain. The other is a hardening effect due to transformation of the hard phase and matrix deformation, which will result in an upward change in the tensile curve [46]. It should be noted that the elongation of the 650 °C annealed HWRed steels obtained in this study is higher than those of other low-C medium-Mn steels [8, 12, 47, 48]. This should be mainly attributed to the enhanced TRIP effect resulting from large austenite volume fractions of the experimental steel during tensile deformation.

5 Conclusions

- (1) An ultrafine-grained (UFG) low-carbon medium-manganese steel was fabricated by heavily warm rolling (HWR) and the subsequent quenching. Compared with hot-rolled and quenched steel, the HWR steel exhibits simultaneous enhancement in uniform elongation, strength and work hardening due to refinement of the martensitic microstructures.
- (2) The HWR steels annealed at lower temperatures below 550 °C and at higher temperatures above 700 °C comprise only α -phase, while ultrafine γ -austenite is formed by reverse transformation when annealing at intermediate temperatures from 550 to 700 °C and the volume fraction increases with increasing annealing temperatures.
- (3) The transformed ultrafine austenite and ferrite remain ~ 500 nm and ~ 800 nm in size when the HWR steel was annealed at 650 and 700 °C for 1 h, respectively, showing an excellent thermal stability.
- (4) The HWR steel annealed at 650 °C exhibited the highest optimal balance of mechanical properties of YS, UTS, TEL and PSE with values ~ 906 MPa, ~ 1011 MPa, $\sim 51\%$ and ~ 52 GPa%, respectively. The extraordinary improvement in mechanical properties is closely associated with the UFG austenite formation in reverse transformation and principally attributed to transformation-induced plasticity (TRIP) effect.

Acknowledgement This work was financially supported by the National Major Science and Technology Project of China (No. 2014ZX07214-002).

References

- [1] H. Aydin, E. Essadiqi, I.H. Jung, S. Yue, *Mater. Sci. Eng. A* **564**, 501 (2013)
- [2] W.Q. Cao, C. Wang, J. Shi, M.Q. Wang, W.J. Hui, H. Dong, *Mater. Sci. Eng. A* **528**, 6661 (2011)
- [3] B.C. De Cooman, P. Gibbs, S. Lee, D.K. Matlock, *Metall. Mater. Trans. A* **44**, 2563 (2013)
- [4] Z.H. Cai, H. Ding, H. Kamoutsi, G.N. Haidemenopoulos, R.D.K. Misra, *Mater. Sci. Eng. A* **654**, 359 (2016)
- [5] Z.H. Cai, B. Cai, H. Ding, Y. Chen, R.D.K. Misra, *Mater. Sci. Eng., A* **676**, 263 (2016)
- [6] Q. Tonizzo, A.F. Gourgues-Lorenzon, M. Mazzière, A. Perlade, I. Zuazo, *Mater. Sci. Eng. A* **706**, 217 (2017)
- [7] Z.H. Cai, H. Ding, R.D.K. Misra, Z.Y. Ying, *Acta Mater.* **84**, 229 (2015)
- [8] Z.C. Li, H. Ding, Z.H. Cai, *Mater. Sci. Eng., A* **639**, 559 (2015)
- [9] Z.H. Cai, H. Ding, R.D.K. Misra, H. Kong, H.Y. Wu, *Mater. Sci. Eng. A* **595**, 86 (2014)
- [10] J. Shi, X. Sun, M. Wang, W. Hui, H. Dong, W. Cao, *Scr. Mater.* **63**, 815 (2010)
- [11] R.L. Miller, *Metall. Trans.* **3**, 905 (1972)
- [12] Y. Zou, Y.B. Xu, Z.P. Hu, X.L. Gu, F. Peng, X.D. Tan, S.Q. Chen, D.T. Han, R.D.K. Misra, G.D. Wang, *Mater. Sci. Eng. A* **675**, 153 (2016)
- [13] Z.H. Cai, H. Ding, X. Xue, J. Jiang, Q.B. Xin, R.D.K. Misra, *Scr. Mater.* **68**, 865 (2013)
- [14] S. Lee, S.J. Lee, B.C. De Cooman, *Scr. Mater.* **65**, 225 (2011)
- [15] H. Yang, H.K.D.H. Bhadeshia, *Scr. Mater.* **60**, 493 (2009)
- [16] E. Bagherpour, M. Reihanian, R. Ebrahimi, *Mater. Des.* **36**, 391 (2012)
- [17] J. Kim, I. Kim, D.H. Shin, *Scr. Mater.* **45**, 421 (2001)
- [18] N.T. Suji, R. Ueji, Y. Minamino, *Scr. Mater.* **47**, 69 (2002)
- [19] Y. Ivanisenko, R.K. Wunderlich, R.Z. Valiev, H.J. Fecht, *Scr. Mater.* **49**, 947 (2003)
- [20] S.H. Sun, A.M. Zhao, R. Ding, X.G. Li, *Acta Metall. Sin. (Engl. Lett.)* **31**, 216 (2018)
- [21] H.Q. Huang, H.S. Di, N. Yan, Y.G. Deng, R.D.K. Misra, J.P. Li, *Acta Metall. Sin. (Engl. Lett.)* **31**, 503 (2018)
- [22] J. Chen, Y. Liu, Y. Xiao, Y. Liu, C. Liu, H. Li, *Acta Metall. Sin. (Engl. Lett.)* **31**, 706 (2018)
- [23] R. Song, D. Ponge, D. Raabe, *Acta Mater.* **53**, 4881 (2005)
- [24] T. Maki, C.M. Wayman, *Metall. Trans. A* **7**, 1511 (1976)
- [25] S.W. Seo, G.S. Jung, J.S. Lee, C.M. Bae, H.K.D.H. Bhadeshia, D.W. Suh, *Mater. Sci. Technol.* **31**, 436 (2015)
- [26] M. Calcagnotto, Y. Adachi, D. Ponge, D. Raabe, *Acta Mater.* **59**, 658 (2011)
- [27] J. Hu, L.X. Du, H. Xie, P. Yu, R.D.K. Misra, *Mater. Sci. Eng. A* **605**, 186 (2014)
- [28] T. Hanamura, S. Torizuka, A. Sunahara, M. Imagumbai, H. Takechi, *ISIJ Int.* **51**, 685 (2011)
- [29] X. Zhao, Y. Shen, L. Qiu, Y. Liu, X. Sun, L. Zuo, *Materials (Basel)* **7**, 7891 (2014)
- [30] R. Zhang, W.Q. Cao, Z.J. Peng, J. Shi, H. Dong, C.X. Huang, *Mater. Sci. Eng. A* **583**, 84 (2013)
- [31] J. Zhang, H. Ding, R.D.K. Misra, C. Wang, *Mater. Sci. Eng. A* **611**, 252 (2014)
- [32] Z. Li, D. Wu, *ISIJ Int.* **46**, 121 (2006)
- [33] J.H. Ryu, J.I. Kim, H.S. Kim, C.S. Oh, H.K.D.H. Bhadeshia, D.W. Suh, *Scr. Mater.* **68**, 933 (2013)
- [34] L. Luo, W. Li, L. Wang, S. Zhou, X. Jin, *Mater. Sci. Eng. A* **682**, 698 (2017)
- [35] Y. Sun, S. Xu, A. Shan, *Mater. Sci. Eng. A* **641**, 181 (2015)
- [36] Z.H. Cai, H. Ding, Z.Y. Tang, R.D.K. Misra, *Mater. Sci. Eng. A* **676**, 289 (2016)
- [37] Y.F. Shen, Y.D. Liu, X. Sun, Y.D. Wang, L. Zuo, R.D.K. Misra, *Mater. Sci. Eng. A* **583**, 1 (2013)
- [38] P. Jacques, Q. Furnémont, A. Mertens, F. Delannay, *Philos. Mag. A* **81**, 1789 (2001)
- [39] X.C. Xiong, B. Chen, M.X. Huang, J.F. Wang, L. Wang, *Scr. Mater.* **68**, 321 (2013)
- [40] J.H. Ryu, D.I. Kim, H.S. Kim, H.K.D.H. Bhadeshia, D.W. Suh, *Scr. Mater.* **63**, 297 (2010)
- [41] C. Wang, W. Cao, J. Shi, C. Huang, H. Dong, *Mater. Sci. Eng. A* **562**, 89 (2013)
- [42] E.O. Hall, *Proc. Phys. Soc.* **643**, 747 (1951)
- [43] Z. Li, L. Fu, B. Fu, A. Shan, *Mater. Sci. Eng. A* **558**, 309 (2012)
- [44] C.H. Cáceres, J.R. Griffiths, A.R. Pakdel, C.J. Davidson, *Mater. Sci. Eng. A* **402**, 258 (2005)
- [45] I. Gutierrez-Urrutia, D. Raabe, *Acta Mater.* **60**, 5791 (2012)
- [46] L.M. Fu, Z.M. Li, H.R. Wang, W. Wang, A.D. Shan, *Scr. Mater.* **67**, 297 (2012)
- [47] D.W. Suh, S.J. Park, T.H. Lee, C.S. Oh, S.J. Kim, *Metall. Mater. Trans. A* **41**, 397 (2009)
- [48] H.F. Xu, J. Zhao, W.Q. Cao, J. Shi, C.Y. Wang, C. Wang, J. Li, H. Dong, *Mater. Sci. Eng. A* **532**, 435 (2012)